Indian Journal of Pure & Applied Physics
Vol. 58, October 2020, pp. 740-749

# Investigation of vacuum evaporated SnTe thin films for their structural, electrical and thermoelectric properties

Praveen Tanwar[a], Sukhvir Singh[a*], A K Panwar[b*] & A K Srivastava[c]

[a]Indian Reference Materials-BND, CSIR - National Physical Laboratory, Dr. K. S. Krishnan Road, New Delhi – 110 012, India
[b]Department of Applied Physics, Delhi Technological University, Shahbad Daulatpur, Main Bawana Road, Delhi – 110 042, India
[c]CSIR-Advanced Materials and Processes Research Institute, Bhopal – 462 064, India

*Received 31 December 2019; accepted 15 September 2020*

Remarkable enhancement in figure-of-merit (ZT) value of p-type Tin Telluride (SnTe) thin films is reported in the present investigations. Under high vacuum conditions, all thin films deposited on the glass substrate by using thermal evaporation technique. Thickness of the thin films were kept 55 and 33 nm. Morphological features and the elemental composition of the thin film were investigated using scanning electron microscopy (SEM) and energy-dispersive spectroscopy (EDS) technique respectively. High-resolution transmission electron microscopy (HRTEM) with selected area electron diffraction (SAED) pattern was used to investigate the microstructure of these thin films. For the identification of crystalline features, phase, and nano-crystallites size in all the thin films, the X-ray diffraction (XRD) technique had played a dominant role. The analysis of the XRD data results in a single-phase cubic structure. Atomic force microscopy (AFM) analysis revealed the 2D and 3D view of variable size grains formed on the glass substrate. Four probes method was used to determine the electrical conductivity of these thin films. Electrical measurements revealed the semi-metallic nature of the SnTe thin films. The thermoelectric measurement analysis revealed that the ZT of the thin films was found to be increased as the thickness of the film enhanced. The maximum value of ZT∼1.0 was obtained at room temperature for the film of thickness 55 nm.

**Keywords:** Tin Telluride; Thin film deposition; Thermoelectric, Characterization techniques; SEM, HRTEM, AFM

## 1 Introduction

In the current scenario, when clean energy harvesting has gained global attention, the process of conversion of energy from heat to electricity and vice-versa has emerged as a dynamic process involving thermoelectric (TE) materials[1-6]. Generally, a semiconductor thermoelectric material prepared by mixing of group IV and VI elements has been used for the conversion of a temperature difference into an electrical voltage[7-10]. Thus, the exploitation of waste heat for the generation of electrical energy is an attractive option. Narrow bandgap semiconductor compounds in the form of bulk and thin films now elicit the attention of the research community. Hence, these TE materials were used by researchers in a variety of fields like optoelectronics, infrared (IR), electronic, near-infrared (NIR) detectors, and other diverse applications[10-15]. Group IV-VI semiconductor compounds have significant applications in IR detectors, thermoelectric devices, etc while most of the studies have been reported based on lead chalcogenides, which are toxic in nature[15-19]. Recently SnTe-based semiconductor materials have received significant attention due to high carrier concentration and p-type characteristics[19-22].

TE systems usually based on eco-friendly and energy conversion technology; but small size, pollutants free condition, high reliability and viability in a wide temperature range is the main advantage of these systems. In TE devices, the efficiency is demonstrated by the non-dimensional relation $ZT = S^2\sigma T/\kappa$, where S denotes as Seebeck coefficient (thermopower), σ represents electrical conductivity, T is the absolute temperature and κ is the thermal conductivity. Therefore, to achieve high TE efficiency from materials, high thermo-power, high electrical, and low thermal conductivity are an essential requirement. Hence to design and develop such materials with desired properties is a great challenge for researchers. To acquire excellent performance of a TE device, the power factor $S^2\sigma$ should be high, whereas minimal thermal conductivity is an essential requirement for such devices. It is well known that engineering of lead chalcogenides and their alloys may provide ZT value up to ~ 2.2 in the temperature range of 235 to 670 °C. However, for maintaining a

*Corresponding author: (E-mail: panwaramar@gmail.com)

safe environment, lead-based materials are usually discouraged[22-27].

Among the semiconductor compound of IV-VI groups SnTe has a narrow bandgap around 0.18 eV at room temperature, and hence it is widely utilized for MIR photodetectors as well as for the TE heat converters[27-30]. Typically, SnTe is Sn-deficit; therefore, it acts as a p-type material. Bulk SnTe comprises a NaCl type cubic crystalline structure (space group ($O_h^5 = Fm\bar{3}m$) similar to PbTe and still played the role of promising TE material because its bulk electronic band configuration smartly resembles that of PbTe[30-35]. Due to the existence of two valence bands phenomenon, the hole density of states played a crucial role in different applications. The electronic band structure of SnTe usually resembles PbTe and PbSe band structure; therefore, it is clear that SnTe has a proper perspective and is used as excellent TE material[35-40]. SnTe thin films belong to topological crystalline insulators (TCI) studied for the nascence of line defects responsible for breaking crystalline isomorphism by the tenseness of film. The compound semiconductor IV-VI having a rock-salt structure is recognized for the sliding surface system under epitaxial and tropical strains creating dislocations at the interface region between film and substrate, which spread along the surface. However, it was observed that the thickness of the thin film and grain dimensions played a remarkable role and notably affected to thermal transport properties and played a dominant role[41-48].

In earlier studies, we have investigated the microstructural, optical, spectroscopic, paramagnetic behavior, electrical measurement, and electronic properties of bulk and thin films of SnTe[23-24]. In the present study we report morphology, microstructure, topology, electrical properties, and thermoelectric behavior of varied thickness of SnTe films deposited by the thermal evaporation technique under high vacuum conditions at room temperature.

## 2 Experimental Details

### 2.1 Synthesis of thin films

Bulk SnTe was prepared by vertical directional solidification (VDS) technique[26] using high purity Tin (Sn, 99.999%) and Tellurium (Te, 99.999%) elements supplied by M/S Alfa Aesar. Both the elements were weighed in a Mettler balance AE 50 with the precision of ± 0.0005 g. Thermal evaporation equipment (Model VT-ACG-03) was used for the deposition of SnTe thin films under a high vacuum environment of the order of $10^{-6}$ mbar for evaporation less than 0.01 gm SnTe bulk was adopted as source material in a molybdenum boat. Freshly cleaved NaCl crystal and glass substrate were used for the deposition of SnTe thin film at a temperature of 300 K in high vacuum conditions. SnTe thin films having thickness 55 and 33 nm had been synthesized at room temperature. To study the microstructure of SnTe thin films the deposition process was performed onto freshly cleaved NaCl crystals. Thin films deposited on glass substrate were used for the determination of electrical parameters. The surface roughness of these thin films was recorded by the atomic force microscope (AFM). Liquid $N_2$ trap was used for anti-contamination during the deposition process. Surface morphology of these thin films was examined by using scanning electron microscope (SEM). Elemental compositional analysis and stoichiometry of the as-deposited thin films was carried by the energy dispersive spectrometer (EDS) system an attachment to SEM.

### 2.2 Characterization

High resolution X-ray diffractometer make PAN Analytical, model X'Pert PRO MRD with CuK$\alpha_1$ radiation was used for GIXRD (grazing incidence X – ray diffraction) measurements of as-grown SnTe thin films. Microstructure, interplanar spacing and lattice fringes of SnTe thin films were recorded by FEI make model Tecnai $G^2$ STWIN F30 high resolution transmission electron microscope (HRTEM) operated at 300 kV accelerating voltage. Surface morphological study and elemental compositional analysis of the thin film were recorded under field emission scanning electron microscope (FEG–SEM) make FEI, model SUPRA V40 accompanying with an energy-dispersive spectrometer (EDS) make Oxford, model Ultim Max respectively. Electrical measurements were performed in the warming cycle after cooling the sample to ~ 10 K through standard Four Probe Method. The Nanoscope IIIa Dimension, 3000 SPM atomic force microscope was employed for surface topology and roughness exploration of thin films. This method makes it possible to investigate nanostructures effectively grown on non-conducting substrates. The AFM measurements were carried out in the dynamic contact mode. Harman method was employed to measure the figure-of-merit (ZT) value of SnTe thin films having varied thicknesses.

## 3 Results and Discussion

### 3.1 XRD analysis

XRD patterns of SnTe thin films onto glass substrate revealed the sharp and well-resolved peaks

of the single-phase SnTe compound with cubic structure of the space group $(O_h^5 = Fm\bar{3}m)$ [24]. The observed values of the lattice parameters matched extensively with the JCPDS file no. 08-0487 indicating the growth of polycrystalline SnTe compound[24]. The most intense diffraction peak could be indexed to the lattice plane (200) while other lattice planes denoted as (220), (420), (222), (400) and (422) has peak intensity in decreasing order. Tables 1 and 2 have shown the crystalline planes, FWHM values, crystallite size, and corresponding interplanar d-spacing values for 55 nm and 33 nm thick SnTe films. From the tables, it is observed that the FWHM value for the thin film having thickness 55 nm is larger than the thin film of thickness 33 nm, but crystallite size was smaller for 55 nm thick film and larger for 33 nm film[24]. This fact has already been reported in the earlier studies[24]. The average crystallite size is found to be around 6 nm for 55 nm thick SnTe film and 13 nm for the thin film of thickness 33 nm. A comparison of average crystallite size and corresponding dominating planes are shown in Table 3. Further, the Rietveld refinement of observed XRD patterns of both the 55 nm and 33 nm thick film of SnTe has been perfomed and shown in Fig. 1 (a) and (b). For the XRD pattern of thin film of thickness 55 nm, Rietveld analysis convergence were reached up to cycle no. 29 leading to parameters R-Factor, R-Expected, DW – statistical and $\chi^2$ values as 5.66, 6.99, 2.008, and 1.12, respectively, with the FWHM parameters (u, v , w) as (0.520, 0.466, -0.340). Hence, on using the shape parameters, X = -0.038, and Y = 0.000, the unit cell parameters of the cubic structure are obtained as a=b=c= 6.289 Å and α=β=γ=90° after Rietveld refinement as shown in Fig. 1(a). Thererfore, the demonstrated Rietveld refinement of 55 nm thick SnTe thin film indicates that the goodness of fitting with almost negligible shifting has been observed at the peak position of (400), (420) and (422) planes except the one very poor intense extra peak belongs to the plane (111) observed at 24.458° resulted in Rietveld refinement. Similarly, for the XRD pattern of thin film of thickness 33 nm, the Rietveld analysis convergence were reached up to cycle no. 15 with R-Factor, R-Expected, DW – statistical and $\chi^2$ values as 5.37, 6.33, 1.816, and 1.19, respectively. The FWHM parameters (u,v,w) are kept as (-0.533, 1.403, 0.031). Therefore, on using the shape parameters: X = -0.026,

Table 1 — Shows the crystalline planes, FWHM values, crystallite size and corresponding interplanar d-spacing values for SnTe thin film of thickness 55 nm deposited on the glass substrate.

| S. No. | 2 θ (degree) | (h k l) | FWHM (β) (degree) | Crystallite Size (D) (Å) | d= nλ/2 Sin θ(Å) |
|---|---|---|---|---|---|
| 1. | 28.425 | (2 0 0) | 1.0181 | 80.7387 | 3.1373 |
| 2. | 40.521 | (2 2 0) | 1.0502 | 80.8945 | 2.2244 |
| 3. | 50.166 | (2 2 2) | 0.9711 | 90.6089 | 1.8169 |
| 4. | 58.734 | (4 0 0) | 2.0263 | 45.1301 | 1.5707 |
| 5. | 66.189 | (4 2 0) | 1.2393 | 76.7485 | 1.4107 |
| 6. | 73.512 | (4 2 2) | 5.0151 | 19.8315 | 1.2872 |

Table 2 — Shows the crystalline planes, FWHM values, crystallite size and corresponding interplanar d-spacing values for SnTe thin film of thickness 33 nm deposited on the glass substrate.

| S. No. | 2 θ (degree) | (h k l) | FWHM (β) (degree) | Crystallite Size (D) (Å) | d= nλ/2 Sin θ (Å) |
|---|---|---|---|---|---|
| 1. | 28.34 | (2 0 0) | 0.5077 | 161.85571 | 3.146 |
| 2. | 40.53 | (2 2 0) | 0.5657 | 150.13003 | 2.223 |
| 3. | 50.19 | (2 2 2) | 0.6946 | 126.67905 | 1.816 |
| 4. | 58.65 | (4 0 0) | 1.1284 | 80.99691 | 1.572 |
| 5. | 66.39 | (4 2 0) | 0.6927 | 137.46446 | 1.406 |
| 6. | 73.65 | (4 2 2) | 0.7685 | 129.54053 | 1.285 |

Table 3 — Comparison of various data of SnTe thin films of thickness 55 nm and 33 nm.

| Thickness of thin film (nm) | Average crystallite size (nm) | Average size of agglomerated grains (nm) | Dominant (hkl) plane | Average Roughnes (nm) |
|---|---|---|---|---|
| 55 | 6 | 125 | (200) | 1.4 |
| 33 | 13 | 120 | (200) | 2.5 |

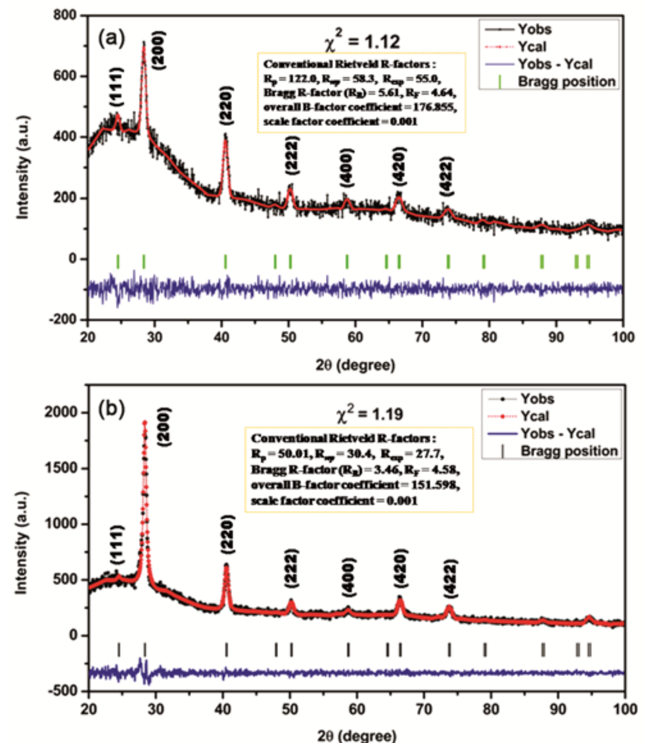


Fig. 1 — Rietveld refinement graph of SnTe thin films of thickness (a) 55 nm, (b) 33 nm, respectively deposited on the glass substrate[24].

and Y = 0.000, the unit cell parameters: a=b=c= 6.293 Å and α=β=γ=90° are estimated after Rietveld refinement as shown in Fig. 1(b). Here, again for the thin film of thickness 33 nm, it has been noticed that the goodness of fitting has indicated the almost negligible shifting for the peak position of (400), (420) and (422) planes. However, one extra peak of very poor intensity is also observed as (111) plane at 24.4362° after refinement.

We have deposited thin films of different thicknesses at room temperature in the range from 33 nm to 275 nm in four attempts and observed that as the thickness of the thin film increases from 55 to 275 nm, the crystallinity was found to increase. Further, it is important to mention here that as the film thickness was reduced from 55 nm to 33 nm, the crystallinity was found to be increased again, which is a noteworthy feature. This interesting behaviour of the film has been reported in our earlier study[24]. The study revealed that there exists a critical thickness (55 nm in the present study), below which if the thickness is further decreased the crystalline nature again prevailed. Figure 2 revealed the dependence of crystallite size on the thickness of the thin film and the effect of critical thickness relation. Earlier researchers[32, 35, 42] have also reported that for a vital thickness of thin film due to substrate, and other deposition parameters, the consequence of strain may be efficacious, but beyond that thickness, the deposited material acts like typical polycrystalline material. These features were considered due to the reduction of the intrinsic micro-strain property in the films and also due to an increase in the crystallite size[24]. But at nano-regime microstructural properties changed, simultaneously other features like micro-strain and dislocation density also altered in a reverse manner. This reversal feature is liable for this unpredicted variation in crystallite size. When the thickness of the thin film was reduced, this unexpected variation was observed for 33 nm, which might be possible due to the high surface to volume ratio of thin films. The crystallite size augmented with the reduction of thin film thickness, and concurrently the strain reduced with the thickness of the films. Further, it is necessary to clarify here that the strain, stress, and instrument broadening on these films have not been measured as the SnTe thin films were not annealed during present investigations.

### 3.2 Morphology and microstructure analysis

FESEM micrographs as shown in Fig. 3(a-b) represents the morphology of SnTe thin films deposited at room temperature on to glass substrate

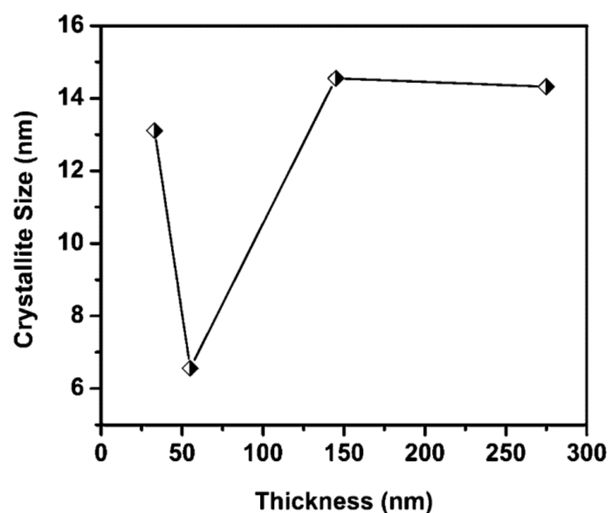


Fig. 2 — Plot showing the relation between crystallite size and SnTe thin films of thickness 275 nm, 145 nm, 55 nm, and 33 nm[24].

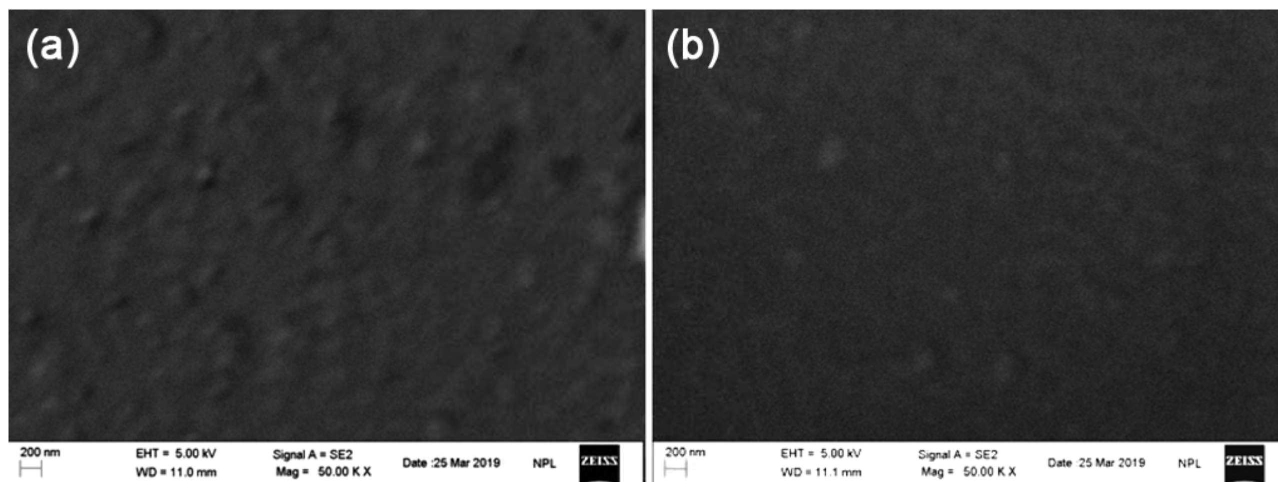


Fig. 3 — FESEM micrographs of SnTe thin films of thickness (a) 55 nm and (b) 33 nm deposited on the glass substrate.

having a thickness of 55 nm and 33 nm, respectively. These micrographs reveal that these thin films are free from any pores and cracks throughout the surface. However, at some places, bubbles like structure are observed and it may be due to stress/ strain developed during the synthesis of the films as depicted in the FESEM images. It may also be due to the thermal instability between the substrate and the deposited film during the thermal deposition process. Since the nano-size polyhedral structures are uniformly distributed, and agglomeration is present at some places, thereby it is difficult to calculate the exact size of grains using the SEM technique. However, the overall grain size shown by SEM images seems to be much higher as compared with XRD results because XRD is used for the estimation of average mean crystallite size, while SEM images represent the size of agglomerated grains consisted of ultra-fine nano-crystallites.

Elemental compositional analysis and stoichiometry of SnTe thin films were performed through the energy dispersive spectrometer (EDS) system an attachment to SEM. The Figs. 4(a) and 4(b) revealed that SnTe thin films exhibit both Sn and Te elements extensively in comparison to any other element. The presence of other elements in the EDS spectra such as sodium (Na), magnesium (Mg), silicon (Si), and aluminum (Al) may be the constituents of the glass substrate.

Microstructural features associated with the SnTe thin films deposited at room temperature were investigated by using the HRTEM technique. HRTEM micrographs, as shown in Fig. 5(a-b) for 55 nm SnTe thick film, revealed the presence of a continuous film having randomly oriented fine crystallites of polyhedral shape. The inset as shown in Fig. 5(a) represents the selected area electron diffraction pattern (SAEDP) of the corresponding area of the film showing ring pattern revealing the polycrystalline nature. Detailed analysis of the SAED pattern (inset) revealed the presence of (200), (220), (222), (400), (420) and (422) oriented lattice planes in the thin film. The observed values of the lattice planes extensively matched with the JCPDS file no. 08-0487 indicating the formation of polycrystalline SnTe compound in the thin film form. Figure 5(b) represents the high-resolution micrograph of the SnTe thin film revealing the lattice planes of agglomerated grains having different sizes throughout the film. The nano-crystallites present in the micrograph are marked as depicted in the figure and the d-spacings of the individual crystallites are indicated as 1.85 Å, 2.23 Å and 3.18 Å that correspond to the planes (222), (220) and (200). Figure 5(c) shows the TEM micrograph of 33 nm thick SnTe film which revealed the smooth, continuous and randomly oriented fine crystallites of SnTe thin film. SAED pattern shown as an inset in the micrograph depicts the presence of rings suggesting the polycrystalline nature of the SnTe thin films. The detailed analysis of the SAED pattern planes with orientation (420), (422), (222), (220), (200) and (110) were revealed. Figure 5(d) demonstrates the lattice fringes of different nanoparticles having d-spacing value 2.22 Å and 3.17 Å which correspond to (220) and (200) planes of SnTe. From the high-resolution micrographs shown in Fig. 5(b, d), it is evident that randomly oriented fine nanoparticles of size 5 nm to 15 nm were found to exist in 55 nm thick film and nanoparticles of size

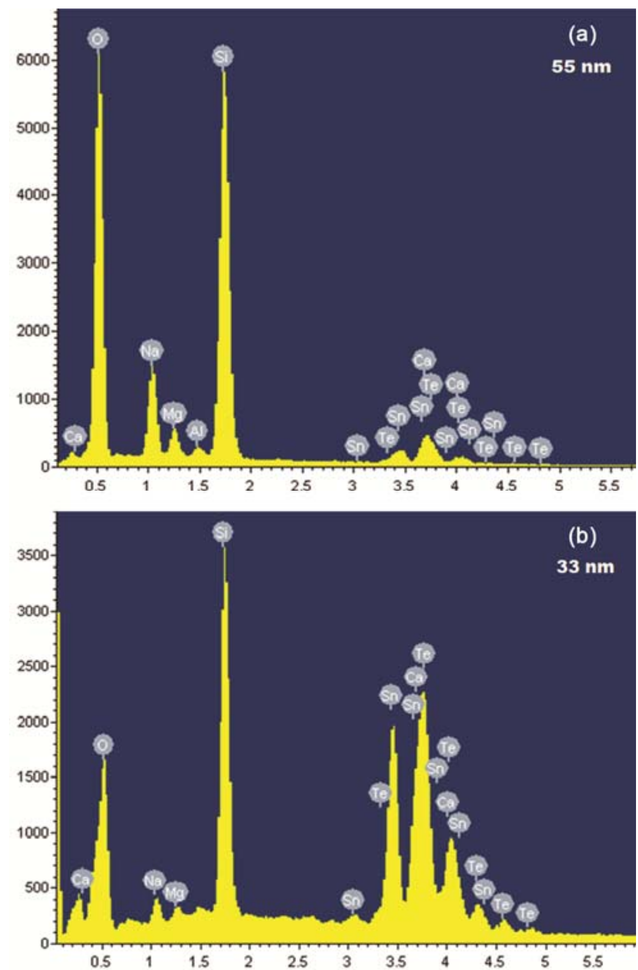


Fig. 4 — EDS spectrum showing presence of various elements in SnTe thin films of the thickness (a) 55 nm and (b) 33 nm.

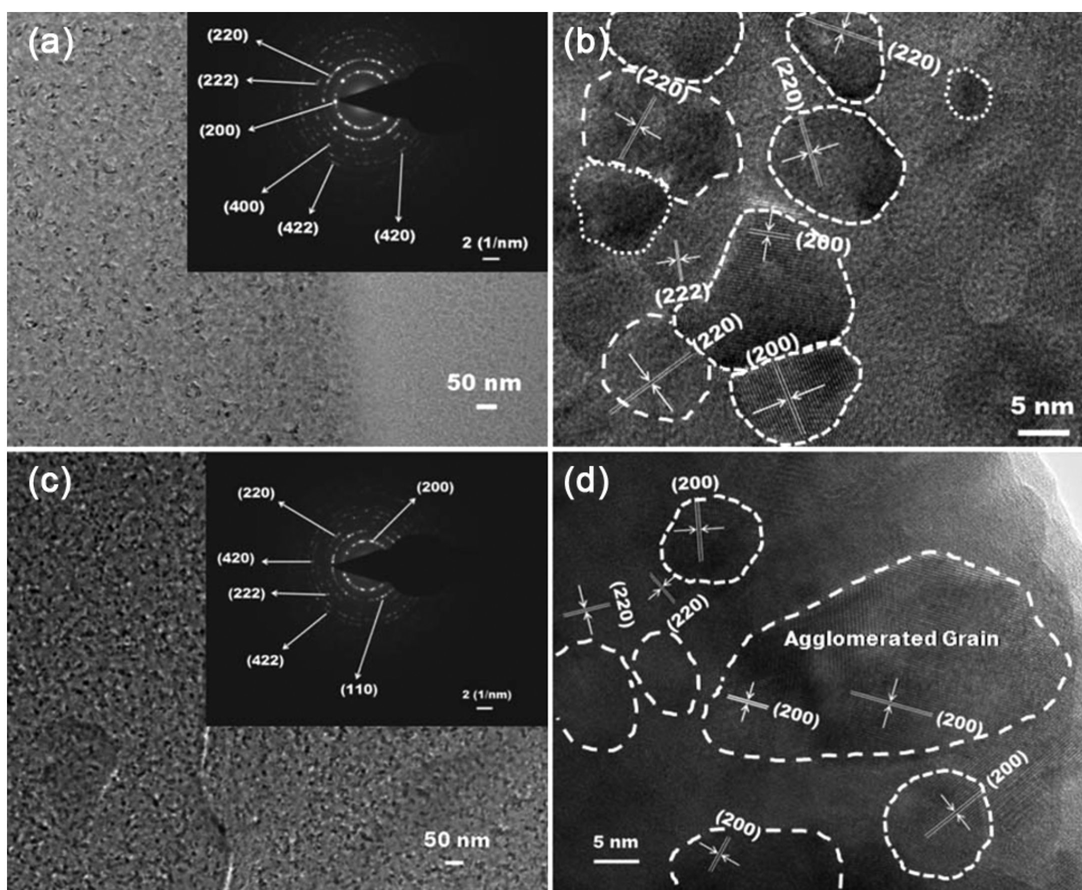


Fig. 5 — TEM micrograph of (a) SnTe thin film of thickness 55 nm and inset represent SAED pattern of corresponding area of the film depicting various planes, (b) HRTEM micrograph revealing various planes exist in SnTe 55 nm thick film. (c) TEM image of SnTe thin film of 33 nm and inset represent the corresponding SAED pattern, (d) HRTEM micrograph of 33nm SnTe thin film showing lattice planes.

varying between 8 nm to 20 nm were found in the SnTe thin film having thickness 33 nm. It is observed that the crystallite size obtained by XRD measurements were found to be in good agreement with crystallite size measured by HRTEM investigations of SnTe thin films. SAED pattern and XRD data are complementary to each other and always in good agreement with each other as a basic requirement in material science. It is right that the different wavelengths of rays used in both techniques are different. The electron beam is used for a SAED pattern because it provides a better resolution. By using two different rays in two different techniques the property of material not changed, d-spacing (inter-planar spacing) remains fixed and both follow Bragg diffraction to match finally with JCPDS file.

### 3.3 AFM analysis

As deposited SnTe thin films of 55 nm and 33 nm thickness were investigated under Atomic force microscopy (AFM). Figure 6 (a-b) indicates the AFM images of 55 nm thick SnTe film grown on a glass substrate showing 2D image 3D images respectively for scanned area 3×3 μm$^2$ in amplitude mode. Most of the grains are seems to be agglomerated in the AFM images. Various surface parameters for 55 nm thick film such as RMS, average roughness, average vertex, surface skewness, and surface kurtosis are found to be 1.9 nm, 1.4 nm, 5.3 nm, 1.4 nm, and 5.6 nm, respectively. Figure 6(c-d) demonstrate the particles of different sizes, but the average size of agglomerated particles is found to be about 125 nm.

The 2D and 3D AFM images of 33 nm thick SnTe film for scanned area 3×3 μm$^2$ are shown in Fig. 7(a-b). The surface parameters of 33 nm SnTe thick film such as RMS, average roughness, average vertex, surface skewness, and surface kurtosis are measured as 3.5 nm, 2.5 nm, 7.6 nm, 1.8 nm, and 9.1 nm, respectively. The surface parameters of 33 nm SnTe thick film such as RMS and average roughness, average vertex, surface skewness, and surface kurtosis are measured as 3.5 nm, 2.5 nm, 7.6 nm, 1.8 nm, and 9.1 nm, respectively.

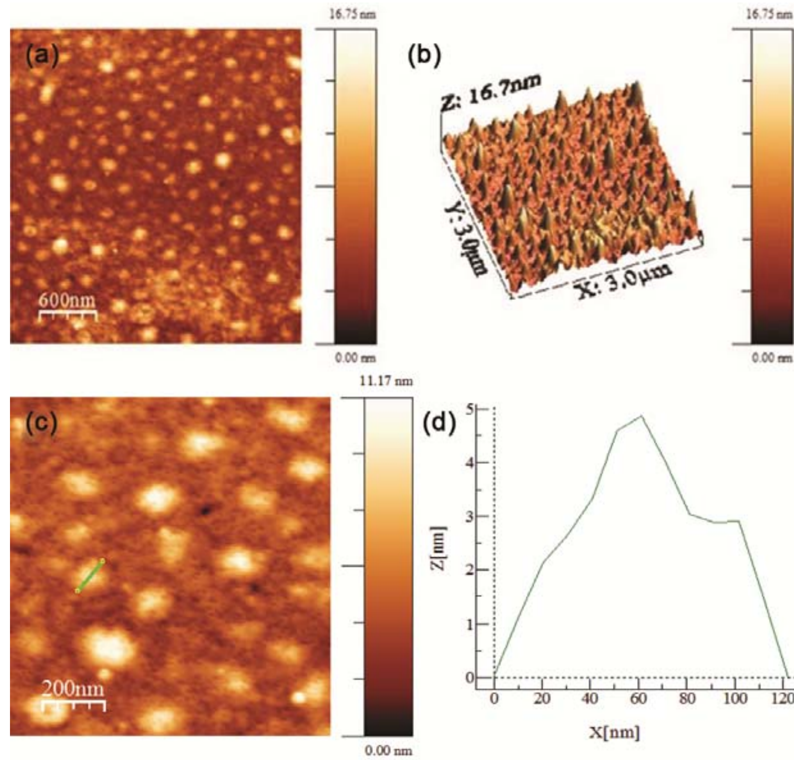


Fig. 6 — AFM images (a) and (b) are 2D and 3D view showing surface roughness, agglomerated particles, and structure of 55 nm thick film and (c) and (d) showing the uniform distribution of agglomerates and measurement of agglomerated particles in the graph, respectively.

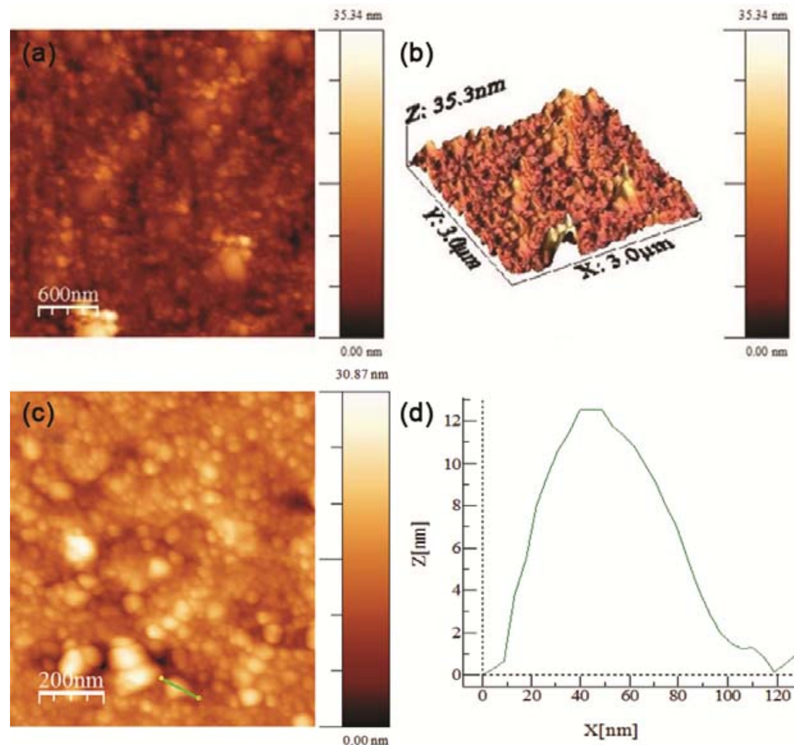


Fig. 7 — AFM images (a) and (b) are 2D and 3D view showing surface roughness, agglomerated particles, and structure of 33 nm thick film. (c) and (d) showing the uniform distribution of agglomerates and measurement of agglomerated particles in the graph, respectively.

AFM images as shown in Fig. 7(c-d) revealed the particles of various shapes and sizes, however, the average size of agglomerated particles is found to be about 120 nm.

**3.4 Electrical properties measurements**

The electrical characteristics of the as-deposited SnTe thin films were measured as a function of temperature from 10 K to 340 K. The P/N type tester was used for the measurement of p-type behavior of as grown SnTe ingot[23]. Resistivity (ρ) versus temperature (T) measurement was conducted in the warming cycle by cooling the sample to the temperature of 10 K. Temperature-dependent resistivity measurement was performed by using a standard four-probe method. Resistivity variation demonstrated the semi-metallic behavior of the sample within the temperature range 10 K to 340 K as depicted in Fig. 8(a-b). For the as-grown bulk SnTe compound, the change in the slope of the resistivity data at 250 K and 25 K has been reported elsewhere[23].

The change in the slope of the resistivity versus temperature data for 55 nm SnTe thin film at 229 K and 80 K is shown in Fig. 8 (a). Whereas the variation in the slope of the resistivity data for 33 nm thin film at 219 K and 55 K is depicted Fig. 8 (b). It may be possible that the electrical conductivity of the SnTe thin films has been changed because of (a) scattering due to isotropic background phenomenon, (b) scattering related to the external surface, and (c) scattering depends on the distribution of planar potentials[15-17, 19-27, 48]. Similar behavior of temperature-dependent resistivity variation for $Pb_{1-x}Sn_xTe$ thin films has also been observed by the researcher[25]. Hence, from the electrical resistivity measurements, it is observed that as the thickness of the SnTe films increases from 33 nm to 55 nm, the electrical resistivity of the thin films was found to decrease. Hence, the present investigations revealed that as the thickness of the SnTe film is reduced, the electrical resistivity of the films is also found to be reduced *i.e* electrical conductivity has increased. It is well-known that SnTe has semi-metallic nature and hence ρ vs T curve will not be a straight line. The main significance of the two slope changes helps to determine the electrical conductivity and bandgap of the material. The working principle and dependence of various parameters behind the ρ-T curve is already described earlier[23-27, 48].

**3.5 Thermoelectric power (ZT) measurements**

In the present study, the ZT measurements of SnTe thin films have been determined by using Harman and thermoelectric Vander Pauw method. Recently Pundir and coworkers reported ZT measurement of $Bi_2Te_3$ nanostructured thin films by using Harman and thermoelectric Vander Pauw method[29]. The speculation of this method is based on two interesting effects that participate in an imperative role in the measurement of TE characteristics of a substance. First is electrical potential difference arising due to the ohmic resistance of the material, and it is proportional to $1/\sigma$. Second is the flow of electrical current that creates a temperature gradient, which is responsible for the rise of a supplementary voltage drop (Seebeck effect). Therefore, the TE involvement due to the voltage drop is proportional to $TS^2/\kappa$. The recently developed concepts such as band energy alteration and defect engineering[30-37] have been utilized to expand the thermoelectric efficiency (ZT) from 0.4 to 1.6. The value of ZT for pristine SnTe was found to be 0.4, but synergetic dominance of band energy modification and defect engineering effectively controlled[38] ZT up to 1.6. A comparison of the

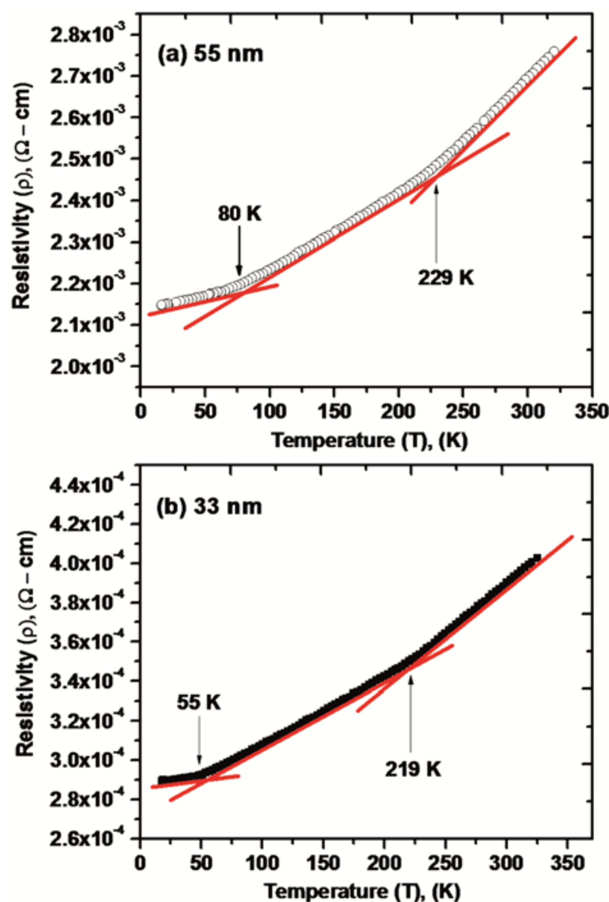


Fig. 8 — (a) and (b) Resistivity vs. Temperature Measurement of SnTe thin films of thickness 55 nm and 33 nm deposited on glass substrate, respectively.

Table 4 — Summarized details of ZT for earlier researchers and our data.

| S. No. | Material details | Type | Temperature (K) | ZT |
|---|---|---|---|---|
| 1. | Pristine SnTe | Undoped | 840 | 0.4 |
| 2. | $Sn_{0.91}Mn_{0.14}Te(Cu_2Te)_{0.05}$ | Alloying | 925 | 1.6 |
| 3. | $Sn_{1-x}Zn_xTe$ (x = 0, 0.01, 0.02, 0.04) | Doped | 775 | 0.5 |
| 4. | $Sn_{0.75+\delta}Ge_{0.05}Cd_{0.2}Te(Cu_2Te)_{0.05}$ | Alloying | 800 | 1.3 |
| 5. | $Sn_{0.86}Mn_{0.14}Te(Cu_2Te)_{0.05}$-5atm%Sn | Doped | 923 | 1.6 |
| 6. | SnTe + 10 mol % $MnO_2$ | Doped | 873 | 1.5 |
| 7. | $Sn_{0.848}Sb_{0.14}In_{0.012}Te$ | Alloying | 800 | 0.8 |
| 8. | *SnTe thin film (55 nm thickness) | Nanostructured thin film | 300 | 1.00 |

**Thin film of SnTe deposited on glass substrate using vacuum evaporation technique*

thermoelectric measurements carried out by earlier researchers on pure and doped bulk SnTe, and SnTe thin films are shown in Table 4. Our ZT measurement data for SnTe thin films is found to be about 1.0 at room temperature is also as shown in Table 4. It is observed that the ZT value of SnTe thin films of thickness 33 nm and 55 nm synthesized on the glass substrate at room using vacuum deposition technique revealed high value as compared to the pristine bulk SnTe and other doped SnTe compound as depicted in Table 4. The figure-of-merit ZT of bulk SnTe material was found reported as 0.4 as shown in Table 4.

## 4 Conclusions

The present investigation on the SnTe thin films has been carried out to understand the thermoelectric properties, morphology, electrical properties, and topological features having a varied thickness of 33 nm and 55 nm. HRXRD measurements revealed that SnTe thin films have polycrystalline features. The average crystallite size of the thin film of thickness 55 nm was found to be smaller as compared to the thin film of thickness 33 nm. However, SEM and AFM measurements show that the average size of agglomerated grains found to be more for the 55 nm thin film. As the thickness of the SnTe film was reduced, the roughness of thin film was found to increase, which may be a reason for the decrease in ZT value. For a relatively higher thickness of the film, it revealed the higher value of ZT. Electrical parameter measurement revealed that P-type SnTe is semi-metallic, and resistivity is temperature-dependent. Due to hopping or tunneling transport at low temperatures, the dependence of electrical conductivity on temperature becomes unretentive. A direct relation between surface roughness and agglomerated grains can explore the fact that surface roughness decreases as the average size of agglomerates increases due to the enhancement of film thickness. The factors mentioned above may result in the reduction of thermal conductivity due to phonon scattering, and consequently, improvement in ZT of thin films might occur.

## Acknowledgment

Authors express their sincere thank to Director, CSIR-National Physical Laboratory, India, for providing the necessary experimental facilities to carry out the research work. In addition authors are thankful to Dr. R. P. Pant, Dr. H. K. Singh, Dr. K. K. Maurya, Mr. Abhisekh Yadav, Dr. J. S. Tawale, Dr. Aashit Patra, Mr. Dinesh Chauhan, Mr. Sandeep Singh, Dr. P. Jain for their support during this whole scientific work.

## References

1 Li J F, Liu W S, Zhao L D & Zhou M, *NPG Asia Mater*, 2 (2010) 152.
2 Erickson A S, Chu J H, Toney M F, Geballe T H & Fisher I R, *Phys Rev B*, 79 (2009) 024520.
3 Salje E K H, Safarik D J, Modic K A, Gubernatis J E, Cooley J C, Taylor R D, Mihaila B, Saxena A, Lookman T & Smith J L, *Phys Rev B*, 82 (2010) 184112.
4 Xia Y, Qian D, Hsieh D, Wray L, Pal A, Lin H, Bansil A, Grauer D, Hor Y S, Cava R J & Hasan M Z, *Nat Phys*, 5 (2009) 398.
5 Tanaka Y, Ren Z, Sato T, Nakayama K, Souma S, Takahashi T, Segawa K & Ando Y, *Nat Phys*, 8 (2012) 800.
6 Safdar M, Wang Q S, Mirza M, Wang Z X, Xu K & He J, *Nano Lett*, 13 (2013) 5344.
7 Zhou M, Gibbs Z M, Wang H, Han Y, Xin C, Li L & Snyder G J, *Phys Chem Chem Phys*, 16 (2014) 20741.
8 Böberl M, Kovalenko M V, Gamerith S, List E J W & Heiss W, *Adv Mater*, 19 (2007) 3574.
9 Ning J, Men K, Xiao G, Zou B, Wang L, Dai Q, Liu B & Zou G, *Cry Eng Commun,* 12 (2010) 4275.
10 Yang Z, Sun Z H, Ming T, Li G S, Wang J F & Yu J C, *J Mater Chem*, 19 (2009) 7002.
11 Malik M A, O'Brien P & Helliwell M, *J Mater Chem*, 15 (2005) 1463.
12 Heremans J P, Wiendlocha B & Chamoire A M, *Ener Environ Sci*, 5 (2012) 5510.
13 Pei Y, Shi X, LaLonde A, Wang H, Chen L & Snyder G J, *Nature*, 473 (2011) 66.

14 Biswas K, He J, Zhang Q, Wang G, Uher C, Dravid V P & Kanatzidis M G, *Nat Chem*, 3 (2011) 160.
15 Zhang Q, Wang H, Liu W, Wang H, Yu B, Zhang Q, Tian Z, Ni G, Lee S, Esfarjani K, Chen G & Ren Z, *Ener Environ Sci*, 5 (2012) 5246.
16 Zhao L D, He J, Wu C I, Hogan T P, Zhou X, Uher C, Dravid V P & Kanatzidis M G, *J Am Chem Soc*, 134 (2012) 7902.
17 Zhang X & Zhao L D, *J Materiomics*, 1 (2015) 92.
18 Zhao L D, Zhang X, Wu H, Tan G, Pei Y, Xiao Y, Chang C, Wu D, Chi H, Zheng L, Gong S, Uher C, He J & Kanatzidis M G, *J Am Chem Soc*, 138 (2016) 2366.
19 Tan G J, Zhao L D, Shi F Y, Doak J W, Lo S H, Sun H, Wolverton C, Dravid V P, Uher C & Kanatzidis M G, *J Am Chem Soc*, 136 (2014) 7006.
20 Zhang Q, Liao B, Lan Y, Lukas K, Liu W, Esfarjani K, Opeil C, Broido D, Chen G & Ren Z, *Proc Nat Aca Sci USA*, 110 (2013) 13261.
21 Zhao L D, Lo S H, Zhang Y, Sun H, Tan G, Uher C, Wolverton C, Dravid V P & Kanatzidis M G, *Nature*, 508 (2014) 373.
22 Singh D J, *Funct Mater Lett*, 3 (2010) 223.
23 Tanwar P, Srivastava A K, Singh S & Panwar A K, *Adv Sci Lett*, 21 (2015) 2855.
24 Tanwar P, Panwar A K, Singh S & Srivastava A K, *Thin Solid Films*, 693 (2020) 137708.
25 Abramof E, Ferreira S O, Rappl P H O, Closs H & Bandeira I N, *J App Phys*, 82 (1997) 2405.
26 Harman T C, *J Appl Phys*, 29 (1958) 1373.
27 Pundir S K, Jain P, Singh S, Srivastava A K & Kumar R, *Adv Sci Eng Med*, 6 (2014) 1006.
28 Pal A K, Mondal A & Chaudhuri S, *Vacuum*, 41 (1990) 1460.
29 Pundir S K, Jain P, Singh S, Srivastava A K & Kumar R, *Adv Sci Eng Med*, 5 (2013) 436.
30 Zhang Q, Cao F, Liu W, Lukas K, Yu B, Chen S, Opeil C, Broido D, Chen G & Ren Z, *J Am Chem Soc*, 134 (2012) 10031.
31 Shen H, Lee S, Kang J G, Eom T Y, Lee H & Han S, *Appl Surf Sci*, 429 (2018) 115.
32 Schreyeck S, Brunner K, Molenkamp L W & Karczewski G, *Phys Rev Mat*, 3 (2019) 024203.
33 Wanarattikan P, Jitthammapirom P, Sakdanuphab R & Sakulkalavek A, *Adv Mater Sci Eng*, 2019 (2019) 6954918.
34 Chen H L, Lu Y M & Hwang W S, *Mater Trans JIM*, 46 (2005) 872.
35 Chen Z, Wang R, Wang G, Zhou X, Wang Z, Yin C, Hu Q, Zhou B, Tang J & Ang R, *Chin Phys B*, 27 (2018) 047202.
36 Khachatryan H, Lee S N, Kim K B & Kim M, *Metals*, 9 (2019) 12.
37 Li W, Chen Z, Lin S, Chang Y, Ge B, Chen Y & Pei Y, *J Materiomics*, 1 (2015) 307.
38 Li W, Wu Y, Lin S, Chen Z, Li J, Zhang X, Zheng L & Pei Y, *ACS Energy Lett*, 2 (2017) 2349.
39 Li S, Li X, Ren Z & Zhang Q, *J Mater Chem A*, 6 (2018) 2432.
40 Moshwan R, Yang L, Zou J & Chen Z G, *Adv Funct Mater*, 27 (2017) 1703278.
41 Orabi R A R A, Hwang J, Lin C C, Gautier R, Fontaine B, Kim W, Rhyee J S, Wee D & Fornari M, *Chem Mater*, 29 (2017) 612.
42 Paula S, Carmen L, Corina O, Cornelia R, Stefan N & Ioan G, *Analele Universităţii de Vest din Timişoara*, LII (2008) 136.
43 Reddy R S, Sreedhar A, Reddy A S & Uthanna S, *Adv Mat Lett*, 3 (2012) 239.
44 Shenoy U S & Bhat D K, *J Mater Chem C*, 7 (2019) 4817.
45 Tang J, Gao B, Lin S, Wang X, Zhang X, Xiong F, Li W, Chen Y & Pei Y, *ACS Energy Lett*, 3 (2018) 1969.
46 Wang T, Wang H, Su W, Zhai J, Wang X, Chen T & Wang C, *J Mater Sci*, 54 (2019) 9049.
47 Zhou Z, Yang J, Jiang Q, Xin J, Li S, Wang X, Lin X, Chen R, Basit A & Chen Q, *Chem Mater*, 31 (2019) 3491.
48 Tanwar P, Panwar A K, Singh S & Srivastava A K, *J Nanosci Nanotechnol*, 20 (2020) 3879.